Investigation on micro-distance dual-wavelength separation using fractional Talbot effect

Yang Lei, Jiang Min, Zhao Ningbo, Xie Hongbo

(Key Laboratory of Optoelectronics Information Technology, Ministry of Education, College of Precision Instrument and Optoelectronics Engineering, Tianjin University, Tianjin 300072, China)

Abstract: Micro-distance spectra splitting is a key technology for compact dual-band imaging system in infrared field. Utilizing the Fresnel diffraction theory and angular spectrum theory, the diffractive properties of dual-wavelength and wide angle light passing through stepped phase grating in fractional Talbot distance were theoretically investigated. A typical scheme of imaging structure based on dual-array detection pixels was set up, where two light beams with different wavelength incident after passing through the stepped phase grating. The numerical simulation shows the splitting results of incident 4 μm and 4.5 μm wavelength light with −30° to 30° angle, including the distribution of luminous intensity, energy and signal-to-noise ratio on dual-array detection pixels. Our results are beneficial not only for designing the compact dual-band optical imaging structure, but also for building up precision spectral separating component.

Key words: stepped phase grating; spectral separation; fractional Talbot effect; mid-infrared band

CLC number: TN29 **Document code:** A **DOI:** 10.3788/IRLA201847.0220003

基于分数泰伯效应的双波长微距分束的研究

杨 磊,江 敏,赵宁波,谢洪波

(天津大学 精密仪器与光电子工程学院 光电信息技术教育部重点实验室,天津 300072)

摘 要: 微距光谱分束是红外领域小型双波段成像系统的关键技术之一。利用菲涅耳衍射理论和角谱理论,研究了双波长和宽角度入射光场通过阶梯光栅在分数泰伯距离下的衍射特性。建立了基于阶梯光栅的双探测阵列成像模型,数值模拟了入射波长分别为 4 μm 和 4.5 μm 的光束在−30°~30°入射角度范围的光栅分束结果,获取了探测面上的发光强度、能量和信噪比等参数值。此文的研究成果可为构建微型双波段成像装置及设计精密光谱分束器件提供理论支持。

关键词: 阶梯相位光栅; 频谱分离; 分数泰伯效应; 中红外波段

收稿日期: 2017−07−05; **修订日期:** 2017−08−03

基金项目: 光电信息技术教育部重点实验室(天津大学)开放基金(2017KFKT007)

作者简介: 杨磊(1982−),讲师,硕士生导师,博士,主要从事高速成像、光学设计及量子光学方面的研究。Email:yanglei@tju.edu.cn

0 Introduction

Nowadays, infrared imaging in combination with spectroscopic techniques has drawn much attention in various scientific aspects ranging from astronomy to biomedical engineering as a useful tools for precise measurement[1-4]. Multispectral imaging technology achieves target enhancement or internal structure recognition relying on the particular spectral features of objects[5-8]. An important infrared spectral region is the mid-infrared 3 −14 μm, as it is the home to vibrational transitions of many important molecules as well as the blackbody emission from biological and mechanical objects over a wide range of temperatures, which contains two atmospheric transmission windows of 3−5 μm and 8−13 μm[9-10].

Dual-band infrared imaging system processes much higher performance than single-band system, which has the ability of combing the evaluation of objects both in spatial and spectral dimensions[11-12]. Therefore, the spectrum of incident light must be divided into two parts by a dichroic beam splitter and then form different channels by filters. In order to obtain the compact size splitter with high efficiency, new methods for designing dual-wavelength separation device are discussed. Since the time of J. Fraunhofer[13], diffraction gratings have been used for light decomposition in a very large number of various applications. Spectral separation gratings as described in this paper project two typical wavelength of mid-infrared band simultaneously into the central diffraction orders of the grating. The starting point for the investigation of this grating is the concept of blazed synthetic phase-only holograms in the form of stepped phase functions[14].

As we know, diffraction of a grating at distances expressed as fractions of the Talbot distance, results in a superimposition of shifted and complex weighted replicas of the original object, which is referred to as the fractional Talbot effect[15-16]. Using this effect can produce a lattice-structured phase-only distribution, to convert a uniform plane wave into many concentrated spots of light of equal intensity[17], with little or no energy loss in the conversion, which is the basic principle of dual-wavelength separation. In its original sense, the effect consists in the reproduction of the lateral field distribution at periodic spatial intervals along the axis of propagation of periodic wave field. Here, it has been studied extensively by means of Fresnel diffraction theory, angular spectrum analysis, and other methods of modern wave optics.

In this paper, we present a general analysis of dual-wavelength separation with certain incident angle based on fractional Talbot effect and the simulation shows its validity. The method showing how the Fresnel diffraction theory and angular spectrum theory combined with fractional Talbot effect principle can be applied to separation of dual-wavelength light wave with wide incident angle is described in detail in Sec. II. More details of the method are given in Sec. III, where a numerical analysis is applied to some examples of light wave incoming on the stepped-phase gratings. Finally, we discuss implications and future directions for this work.

1 Theoretical model

It is the purpose of this section to research on a one-dimensional Fresnel diffraction from a periodic grating and the corresponding fractional Talbot effect according to the Fresnel diffraction theory and angular spectrum theory. We start by utilizing simple model to describe the inputting light wave due to any complex wave field can be expressed by linear combination of the spherical wave. Based on the spherical wave and plane wave diffraction theory, it is believed that calculating the Fresnel diffraction should get same results when we use Huygens-Fresnel principle or Fourier plane wave theory. Therefore, by drawing the angle parameter into the angular spectrum, complex wavefront with wide incident angle is equivalent to superposition of plane wave with single incident angle.

To simplify the mathematical deduction process, this article only discusses light separating process for one-dimensional incident light with wide angle, where the stepped phase grating is used as the device for splitting light (shown in Fig.1(a)). Compared with other phase gratings, the stepped phase grating conceptually consists of a number of steps with widths close to the wavelength of the diffracted light, and the transmittance function as given by V. Arrizon[15,18], is

$$t(x)=\left[\mathrm{rect}\left(\frac{x}{d}\right)\exp(i\phi)\right]\cdot\frac{1}{d}\mathrm{comb}\left(\frac{x}{d}\right) \tag{1}$$

where symbol $(\cdot)$ represents convolution integral, $\phi=k\ (n-1)$, n represents the refractive index of grating and k is wave vector of input light wave.

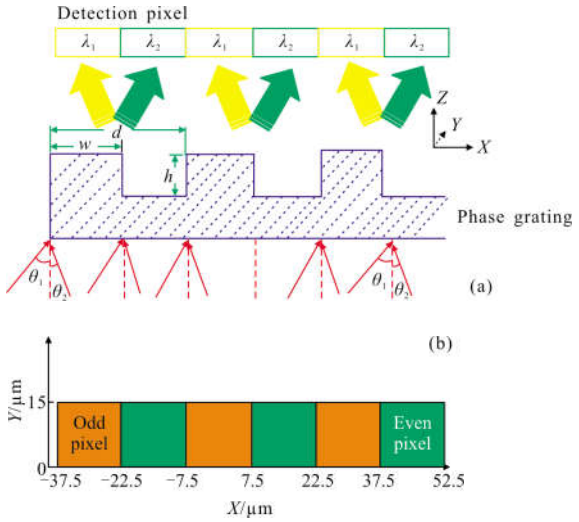

Fig.1 Diagram of imaging structure based on dual-array detection pixels. (a) General view of phase grating separates two beams with wavelength λ_1 and λ_2 in mid-infrared band, in which incident angle is from θ_1 to θ_2. (b) Coordinate system of detection pixels, which is divided into odd pixels ($-7.5\ \mu m+30\cdot l\ \mu m\leqslant x\leqslant 7.5\ \mu m+30\cdot l\ \mu m$, l is an integer) and even pixels ($7.5\ \mu m+30\cdot l\ \mu m\leqslant x\leqslant 22.5\ \mu m+30\cdot l\ \mu m$), respectively

$t(x)$ can also be expressed as a Fourier series

$$t(x)=C_1\exp(i2\pi f_x x) \tag{2}$$

where f_x denotes the angle spectrum of grating and $C_1=\sum_{l=-\infty}^{\infty}[d g\mathrm{sinc}[l\cdot g]\exp[i\phi]]$. In coefficient C_1, the variables are defined as follows: $g=\omega/d$ is the duty ratio of grating, d is grating constant, ω is the width of step, and l represents the number of grating period.

According to the Fresnel approximation, one-dimensional plane wave propagating factor is always written as $\exp(ikz)\exp(-i\pi\lambda z f_x^2)$ (z denoting propagating distance), where the previous item represents propagating factor and the last item represents phase factor. It is straightforward to see that in the determining plane, as an constant value, $\exp(ikz)$ can be ignored in our analysis. For the phase factor, angular spectrum of plane wave with single incident angle is given by $f_x=1\cos\theta/d$, where θ represents incident angle ranging from θ_1 to θ_2.

Considering the angular spectrum, the complex amplitude distribution of outputting plane wave becomes

$$t(x)=C_n\exp\left[\frac{i2\pi l\cos(\theta)x}{d}\right]\cos(\theta) \tag{3}$$

The propagation factor of wave field propagating from surface of grating ($z=0$) to z is

$$v(z,f)=\exp(-i\pi\lambda z f^2) \tag{4}$$

After inverse Fourier transforming the product of wave propagating factor and wave field distribution of complex amplitude, we can obtain the amplitude distribution of diffraction plane, which shows

$$u(x,z)=\int_{-\infty}^{\infty}T(f)v(z,f)\exp(i2\pi fx)\mathrm{d}f \tag{5}$$

where $T(f)$ is the Fourier transform of transmittance function of wave field $t(x)$

$$T(f)=C_1\delta\left[f-\frac{l\cos(\theta)}{d}\right]\cos(\theta) \tag{6}$$

By filtered with sampling function, wave field distribution $u(x)$ can be shown as

$$u(x,z)=\sum_{l=-\infty}^{l=\infty}b_1\exp(i\phi)\exp[-i2\pi l^2 z/Z_T\cos(\theta)]\times \exp[i2\pi xl/d\cos(\theta)]\cos(\theta) \tag{7}$$

where $b_1=\frac{\omega}{d}\ \mathrm{sinc}\left[\frac{l\omega}{d}\right]$ and Z_T is equal to $2d^2/\lambda$ representing Talbot distance.

Furthermore, it is also convenient to observe that a lateral shift of $d/2$, along the x direction, is equivalent to a shift of $Z_T/2$ along the z axis. That is,

$$u(x+d/2,z)=u(x,z+Z_T/2) \tag{8}$$

which illustrate the function $u(x)$ having a transverse

cycle ad and even symmetry.

Considering the superposition of multi-angle incident plane wave, Eq.(7) can be expressed as

$$u(x,z,\theta,\lambda)=\sum_{\theta_1}^{\theta_2}\sum_{l=-\infty}^{l=\infty} b_l\exp(i\phi)\exp[-i2\pi l^2 z/Z_T\cos(\theta)]\times \exp[-i2\pi xl/d\cos(\theta)]\cos(\theta) \quad (9)$$

which is a comprehensive expression of diffractive field from grating.

The Sinc function in Eq. (9) represents the diffractive field formed by single step, when standard rectangular wave field can be composed by superposition of numerous sampling function. Additionally, the broadening of rectangular wave field can be managed by the duty ratio g of grating, due to the reason that the bandwidth of sampling function is always determined by duty ratio g. For the equidistant separation of dual-wavelength case shown in Fig.1(a), the duty ratio g=1/2 is a reasonable choice. $\varphi=2\pi(n-1)h/\lambda$ is the function of step height h and wavelength λ, whose value does not vary with x in the detection plane. In order to achieve the 1/2 duty cycle of imaging plane, φ should be taken $\pi/2$ in our stepped phase grating. The main purpose of the function $\exp\left[-i\pi\lambda z\frac{n^2}{d^2}\cos^2\theta\right]$ in Eq.(9) is to correct the parameter of wave field along the z-axis direction, which is able to take the fixed value when the z plane and incident angle are both determined. The grating period is set at 30 μm, which corresponds to one odd pixel (-7.5 μm$+30\cdot l$ μm$\leqslant x\leqslant 7.5$ μm$+30\cdot l$ μm, l is an integer) and one even pixel (7.5 μm $+$ $30\cdot l$ μm$\leqslant x\leqslant 22.5$ μm$+30\cdot l$ μm) in image plane (Shown in Fig.1(b)).

As a light separation device for imaging system, we are more concerned about the energy of light wave falling into the odd and even pixels. Therefore, we respectively define the energy of light wave incoming on the surface of an odd and even detection pixel as follows

$$E_{odd}(x,z,\theta,\lambda)=\int_{0\ \mu m}^{15\ \mu m}\int_{(-7.5+30\cdot 1)\ \mu m}^{(7.5+30\cdot 1)\ \mu m}\int_{\theta_1}^{\theta_2}|U(x,z,\theta,\lambda)\cos\theta|^2 \mathrm{d}y\mathrm{d}x\mathrm{d}\theta \quad (10)$$

$$E_{even}(x,z,\theta,\lambda)=\int_{0\ \mu m}^{15\ \mu m}\int_{(-7.5+30\cdot 1)\ \mu m}^{(22.5+30\cdot 1)\ \mu m}\int_{\theta_1}^{\theta_2}|U(x,z,\theta,\lambda)\cos\theta|^2 \mathrm{d}y\mathrm{d}x\mathrm{d}\theta \quad (11)$$

Another parameter we focus on is signal-to-noise ratio (SNR) of outputting light falling on odd pixels and even pixels, which illustrates the splitting effect of device. We define the ratio of energy of light wave with wavelength λ_1 (signal) to energy of light wave with wavelength λ_2 (noise) incoming on the surface of an odd detection pixel, which can be expressed as

$$\mathrm{SNR}_{odd}=\frac{E_{odd}(\lambda_1)}{E_{odd}(\lambda_2)} \quad (12)$$

Meanwhile, the ratio of energy of light wave with wavelength λ_2 (signal) to energy of light wave with wavelength λ_1 (noise) incoming on the surface of an even detection pixel can be expressed as

$$\mathrm{SNR}_{even}=\frac{E_{even}(\lambda_1)}{E_{even}(\lambda_2)} \quad (13)$$

In this section, we have presented the basic theory of light wave separation using stepped phase grating in the fractional Talbot distance. We first consider the analytical expression of light wave passing through the stepped phase grating with multi incident angle. We next consider the light splitting effect in our designed grating, including the energy of light falling on detection pixels and signal-to-noise ratio of odd pixels and even pixels, respectively.

2 Results and analysis

The aim of this section is to show that the effect of light separation with dual-wavelength(λ_1=4 μm and λ_2=4.5 μm) plane wave illumination, when the parameters of grating is d=30 μm and g=0.5. Z_{T1} and Z_{T2}, denoting the Talbot distance of light with wavelength λ_1 and λ_2, are 450 μm and 400 μm, respectively. We consider the best case is all the light with wavelength λ_1 incoming on odd pixels and all the light with wavelength λ_2 incoming on even pixels, simultaneously.

We will now test the approach presented in the previous sections by considering some simple cases of incident light, including the case of vertically incident light, single angle incident light and wide angle incident light. The parameters of typical infrared optical we selected, including F number $F\#$=2, focal

length f=160 mm, field of view ω=2.2° and wavelength of incident light in the range of 3.7−4.8 μm, decide the biggest angle of incident light approach to 30°.

The examples of numerical simulation are as follows, including vertically incident light, single angle incident light and wide angle incident light.

2.1 Vertically incident light

In this subsection, we give a simple assumption that light in mid-infrared band is vertically incoming on grating. The distribution of light intensity(λ_1=4 μm) along the x axis is represented in Fig.2. It is made of (a)−(f) figures, whose propagation distance z varies from 0 to Z_{T1}. The showing of Fig.2 (a) and Fig.2(e), z=0 and $z=Z_{T1}/2$, prove the characteristics of $u(x,z)$ written in Eq.(7). We also found that the style of Fig.2(a) and Fig.2(h) is identical, when the parameter

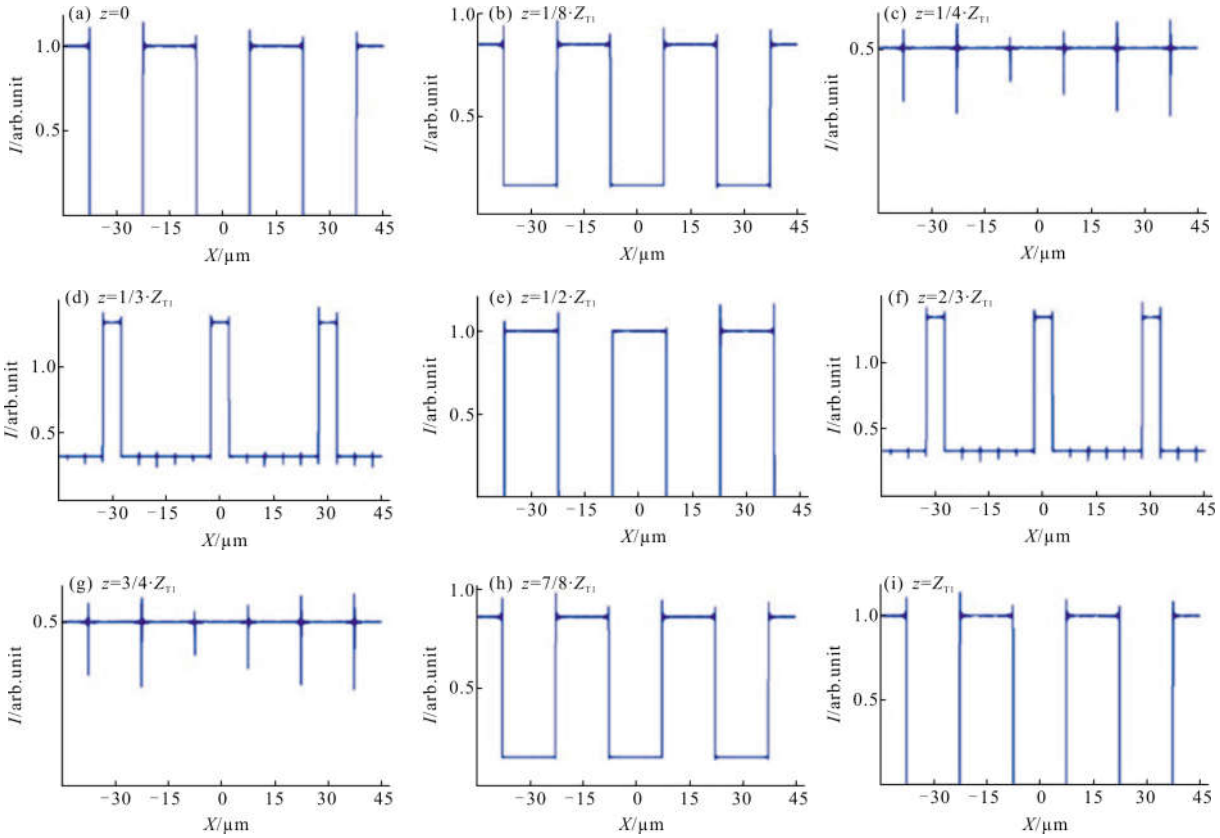

Fig.2 Relative intensity I versus pixel coordinate x, when light wave (λ_1=4 μm) vertically incident in surface of grating (θ=0°). In the picture (a)−(f), we varied the propagating distance z from 0 to Z_{T1}

z=0 changed to $z=Z_{T1}$.

The cases we are more concerned about is the regulation of energy fell onto the detection pixels, whose area is exact 15 μm×15 μm no matter odd pixel or even pixel. In Fig.3, the energy of light detected E versus the propagation z are plotted, when the Fig.3(a) and Fig.3(b) are related to odd pixels and even pixels, respectively. We also observed that the energy of light with wavelength λ_1(solid line) and λ_2 (dotted line) changes with period of Z_{T1} and Z_{T2}, respectively. It is also worth noting that the position

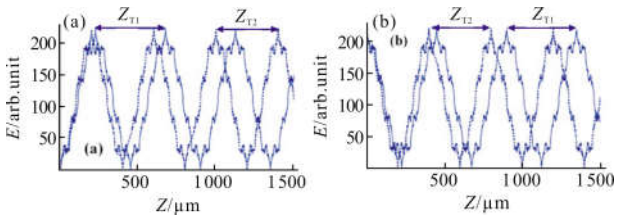

Fig.3 (a) Energy of light wave incoming on the surface of an odd detection pixel Eodd versus the propagating distance z, (b) energy of light wave incoming on the surface of an even detection pixel E_{even} versus the propagating distance z. The solid line represents the energy from light wave with wavelength λ_1, the dashed line represents the energy from light wave with wavelength λ_2

appearing the maximum value of solid curve occurs a deviation from the position appearing the minimum value of dotted curve due to the different value of Z_{T1} and Z_{T2}, which will bring a little difficulties for choosing the optimal z value for completely separating dual-wavelength light wave.

A plot of the SNR of detection pixels as a function of distance z is given in Fig.4, where the light with wavelength λ_1 and λ_2 represents the signal and noise of odd pixel, respectively, vice versa. As shown in Fig.3, the maximum of SNR commonly depends on the minimum noise value of energy on pixels and where it appears. Fig.4 also shows the locations of maximum SNR of odd and even pixels are different, where the value of maximum SNR approach to 100 and 200, respectively. We now want to find the best SNR of odd pixels and even pixels whose z value is around the 1 140 μm, and its value is about 10.

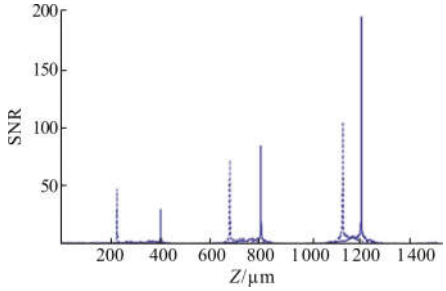

Fig.4 Signal-to-noise ratio of detection pixels. Solid line and dashed line represent the value of SNR_{odd} and SNR_{even}, respectively

2.2 Single angle incident light

In this case, another example that we can mention is the light wave incident with 10°, 20° and 30° incident angles. We will now test the approach presented in the previous sections by describing the regular of light intensity, energy distribution and signal-to-noise ratio after light wave passing through stepped gratings. Figure 5 shows one-dimensional spatial distribution characteristics of relative light intensity in various fractional Talbot distances.

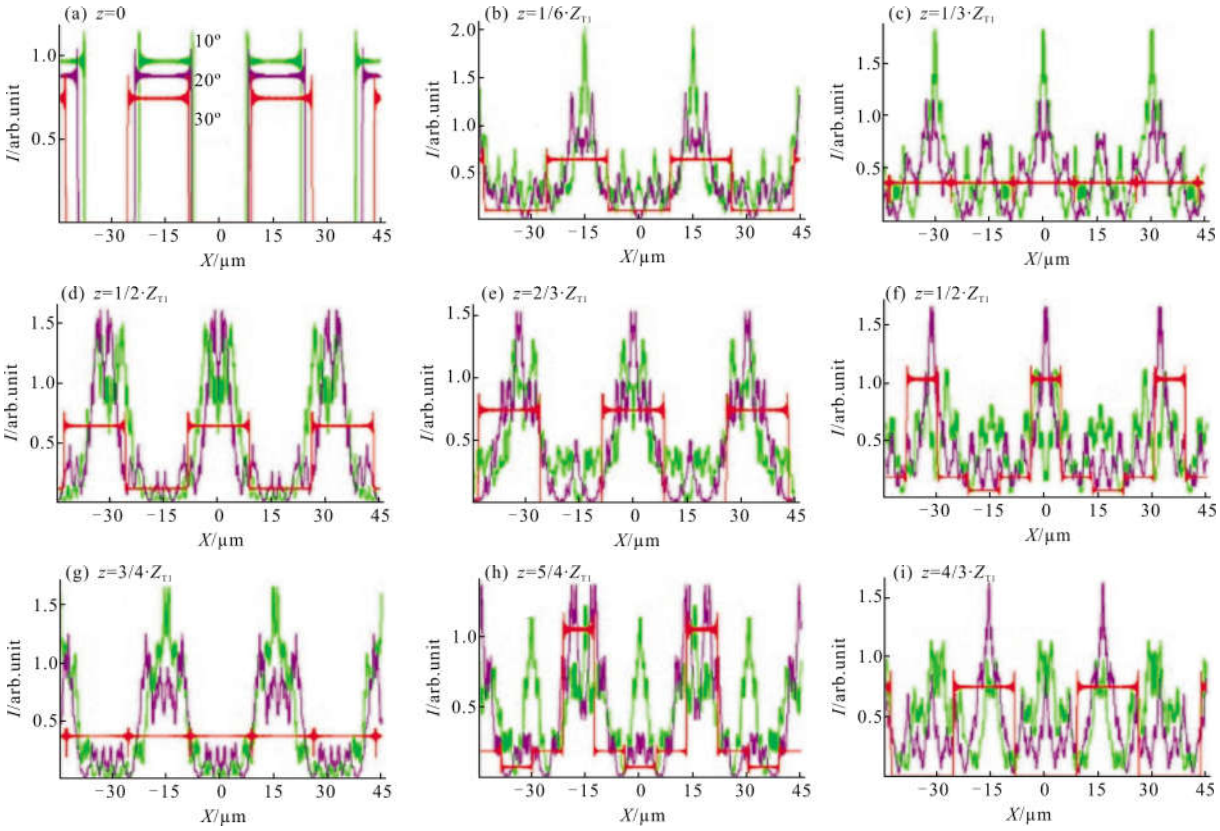

Fig.5 Relative intensity I versus pixel coordinate x, when incident angle of light wave (λ_1=4 μm) is fixed at θ= 10° (green solid line), θ= 20° (purple solid line) and θ=30° (red solid line), respectively. In the picture (a)–(f), we varied the propagating distance z from 0 to $4/3\cdot Z_{T1}$

According to the results shown, we found that various incident angles have different properties, and light wave with 30° have the identical one-dimensional spatial distribution while the z=0 and z=4/3·Z_{T1}.

It is worth noting that, in view of Fig.6, energy of light wave incoming on the surface of an odd (even) pixel varied by specific period, while the period of incident light with 30° has the maximum value. The amplitude of curve is sorted as, 10° incident light is biggest, 20° incident light is second and 30° incident light is smallest.

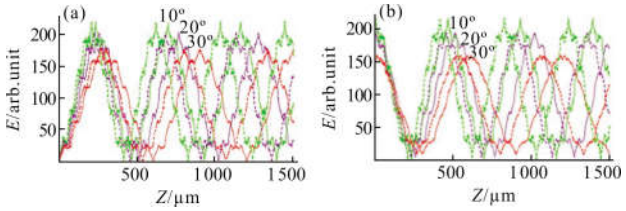

Fig.6 (a) Energy of light wave incoming on the surface of an odd detection pixel E_{odd} versus the propagating distance z; (b) energy of light wave incoming on the surface of an even detection pixel E_{even} versus the propagating distance z. The solid line, purple line and line represents the energy from λ_1 wavelength light wave with 10°, 20° and 30° incident angle, respectively. The dashed green line, purple line and red line represents the energy from λ_2 wavelength light wave with 10°, 20° and 30° incident angle, respectively

Let us then examine the signal-to-noise ratio case (Fig.7), when the light incident angle at 10°, 20° and 30°, respectively. In Fig.7(a), the value of $SNR_{odd(even)}$ has the similar style of curve shown in Fig.4, whose maximum value approaches to 200 and has very small bandwidth. However, in Fig.7(b) and Fig.7(c), the value of SNR_{even} tends to decrease when the incident angle fixed at 20° and 30°, respectively. We can draw a conclusion that the value of SNR_{odd} and SNR_{even} become imbalanced with the increase of the incident angle, which is very unfavorable for light splitted by stepped phase gratings.

2.3 Wide angle incident light

In this subsection, three important properties of the splitted light wave when the incident angle ranging from −30° to 30° are investigated. Compared to curves of light wave with 0° incident angle (Fig.2) and 10° incident angle (Fig.5 (a)), the relative intensity I with multi incident angle as a function of coordinate x is relative complicated. We just find that the curves in Fig. 8(c) and Fig. 8(f) are similar, when the difference of value z is 5/12·Z_{T1}. In addition, we also find the π phase difference between Fig. 8(d) and Fig. 8(g), when the difference of z value is 1/2·Z_{T1}.

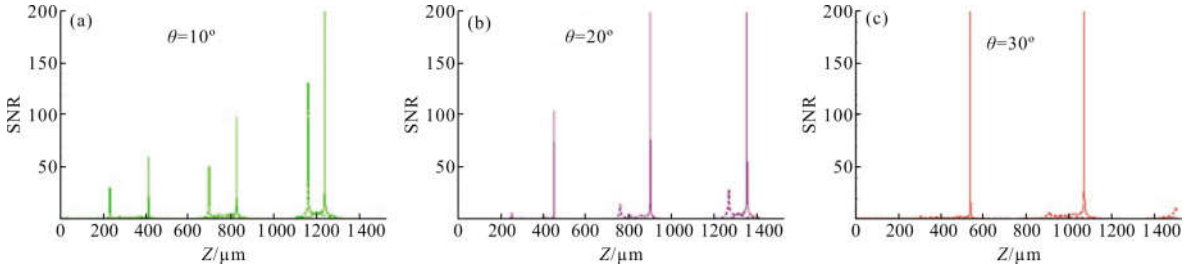

Fig.7 Signal-to-noise ratio of detection pixels, with 10°(Fig.7(a)), 20°(Fig.7(b)) and 30°(Fig.7(c)) incident angle, respectively. In each picture, the solid line represents the value of SNR_{odd}, while the dashed line represents the value of SNR_{even}.

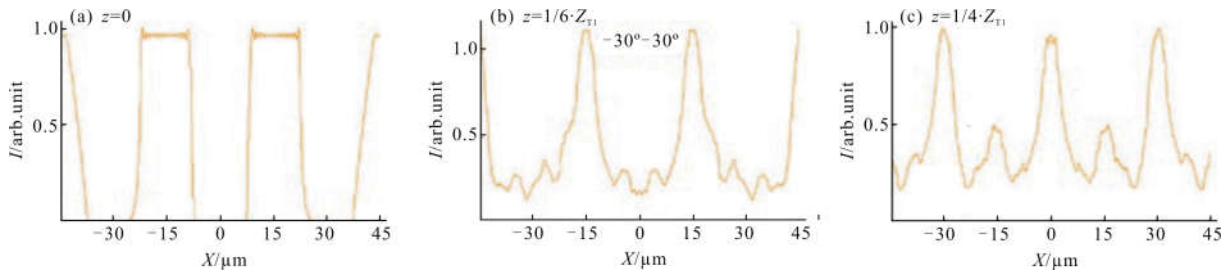

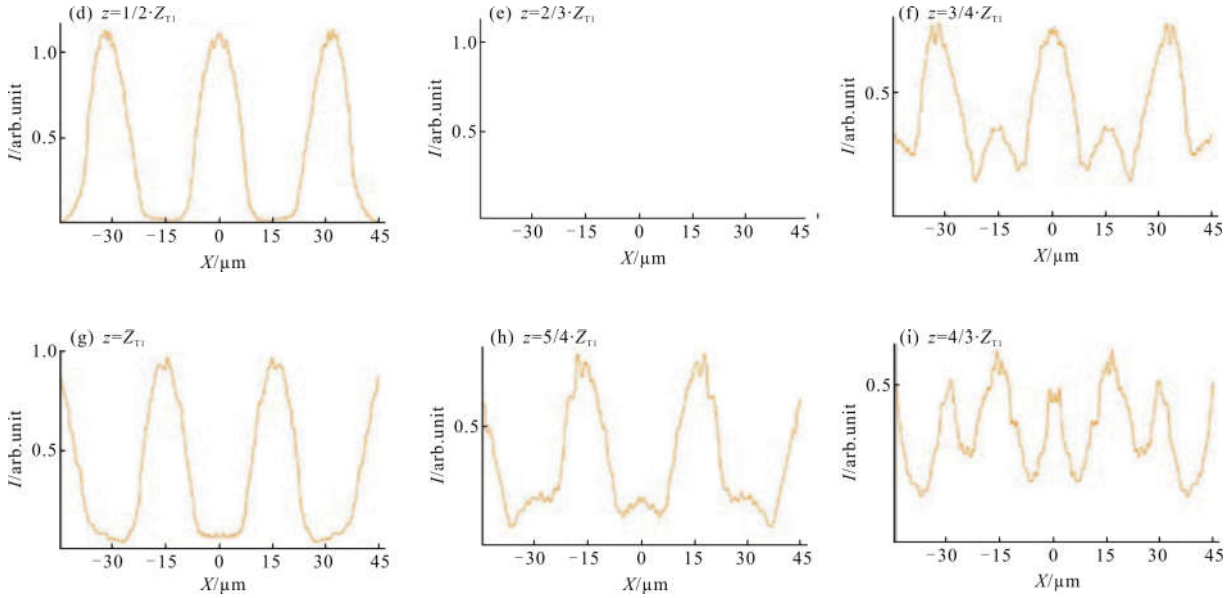

Fig.8 Relative intensity I versus detection pixel coordinate x, when incident angle of light wave ($\lambda 1=4$ μm) ranging from $\theta=-30°$ to $\theta=30°$. In the pictures (a)–(f), we varied the propagating distance z from 0 to $4/3\cdot Z_{T1}$

Fig.9 clearly gives that energy of light wave incoming on the surface of an odd (even) detection pixels $E_{odd(even)}$ varying in the period of Talbot distances Z_{T1} and Z_{T2}. However, as the distance z becomes large, the amplitudes of $E_{odd(even)}$ decreases continuously, which illustrates the effect of spectral separation effect becomes poor at the condition of multi-angle incident light. On the other hand, the best value of SNR_{odd} and SNR_{even} approximately reduce to 4 due to the mixing of different angles of incident light (Shown in Fig.10).

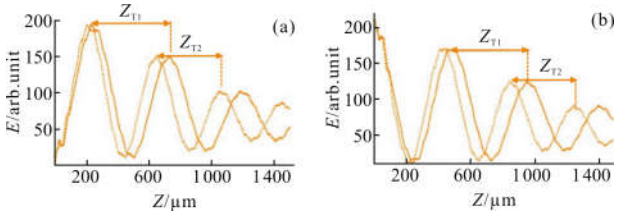

Fig.9 (a) With incident angle ranging from −30° to 30°, energy of light wave incoming on the surface of an odd detection pixel E_{odd} versus the propagating distance z; (b) with incident angle ranging from −30° to 30°, energy of light wave incoming on the surface of an even detection pixel E_{even} versus the propagating distance z. The solid orange line and dashed orange line represents the energy from λ_1 wavelength and λ_2 wavelength light wave, respectively

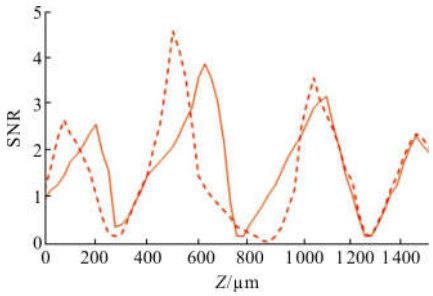

Fig.10 Signal-to-noise ratio of detection pixels when the incident angle of light wave ranging from −30° to 30°. Solid and dashed orange line represents the curve of SNR_{odd} and SNR_{even}, respectively

3 Conclusion

In summary, we have theoretically presented spectral separation properties of stepped phase grating under wide incident angle conditions. Some interesting properties which were not pay close attention before being found, including intensity and energy distribution of light field and signal-to-noise ratio of detection pixels along the propagation direction in micro-distance. Numerical simulation results show the validity of fractional Talbot effect used for separating light with high isolates degree, although the optimum

fractional Talbot distance should be chosen.

A main field of application of the spectral separation gratings may be the multi-spectral imaging technologies. Applications may also be found in the general field of spectrographic analysis and spectrum measurement. And we also suggest that the application of field relating to a variety of areas within diffractive optics promises accurate analysis and high-performance designs.

References:

[1] Labadie L, Wallner O. Mid-infrared guided optics: a perspective for astronomical instruments [J]. ***Optics Express***, 2009, 17(3): 1947-1962.

[2] Wang W Q, Jia X H, Han Y M, et al. Infrared imaging modeling and simulation of DIRCM Laser [J]. ***Infrared and Laser Engineering***, 2016, 45(6): 0606005. (in Chinese)

[3] Li H, Yan C X, Yu P, et al. Measurement of modulation transfer function for IR imaging system [J]. ***Optics and Precision Engineering***, 2016, 24(4): 698-708. (in Chinese)

[4] Huo J, Li M F, Yang R, et al. High sensitive near infrared imaging system based on single element detectors [J]. ***Infrared and Laser Engineering***, 2016, 45 (S1): S104001. (in Chinese)

[5] Kanaev A V, Kutteruf M R, Yetzbacher M K, et al. Imaging with multi-spectral mosaic-array cameras [J]. ***Applied Optics***, 2015, 54(31): F149-F157.

[6] Rueda H, Lau D, Arce G R. Multi-spectral compressive snapshot imaging using RGB image sensors [J]. ***Optics Express***, 2015, 23(9): 12207-12221.

[7] Hou Q Y, Zhang S Q. Design of optical system of multi-spectral imaging system with single detector [J]. ***Infrared and Laser Engineering***, 2015, 44(5): 1638-1642. (in Chinese)

[8] Zhang Y C, Zhao J. Application of improved C-V segmentation in multi-spectral imager [J]. ***Chinese Optics***, 2015, 8(1): 68-73.

[9] Yao J M, Zhang B, Yin K, et al. Mid-infrared supercontinuum generation based on cascaded Raman scattering in a few-mode As_2S_3 fiber pumped by a thulium-doped fiber laser [J]. ***Optics Express***, 2016, 24(13): 14717-14724.

[10] Li C, Xie J J, Pan Q K, et al. Progress of mid-infrared optical parametric oscillator [J]. ***Chinese Optics***, 2016, 9(6): 615-624. (in Chinese)

[11] Kray S, Spoler F, Forst M, et al. High-resolution simultaneous dual-band spectral domain optical coherence tomography [J]. ***Optics Letters***, 2009, 34(13): 1970-1972.

[12] Bai Y, Liao Z Y, Liao S, et al. Infrared dual band athermal optical system with common aperture [J]. ***Optics and Precision Engineering***, 2016, 24(2): 268-277. (in Chinese)

[13] Lemmi C, Ledesma S. Fraunhofer diffraction patterns generated by mixed Cantor gratings [J]. ***Optics Communications***, 1994, 112(1-2): 1-8.

[14] Sheng Y L, Sun L. Near-field diffraction of irregular phase gratings with multiple phase-shifts [J]. ***Optics Express***, 2005, 13(16): 6111-6116.

[15] Arrizon V, Ojeda-Castaneda J. Talbot array illuminators with binary phase gratings [J]. ***Optics Letters***, 1993, 18(1): 1-3.

[16] Banaszek K, Wodkiewicz K, Schleich W P. Fractional Talbot effect in phase space: A compact summation formula [J]. ***Optics Express***, 1998, 2(5): 169-172.

[17] Da X Y. Talbot effect and the array illuminators that are based on it [J]. ***Applied Optics***, 1992, 31(16): 2983-2986.

[18] Szwaykowski P, Arrizon V. Talbot array illuminator with multilevel phase gratings [J]. ***Applied Optics***, 1993, 32(7): 1109-1114.